Journal of Applied Polymer Science

Hybrid Polydiacetylene/Magnetite Nanoparticles: Sensing for Sodium Cetyltrimethylammonium Bromide and Streptavidin

Shengguo Lu,[1] Fang Luo,[1] Xujia Duan,[1] Chen Jia,[1] Yuwang Han,[2] He Huang[1]

[1]State Key Laboratory of Materials-Oriented Chemical Engineering, College of Biotechnology and Pharmaceutical Engineering, Nanjing University of Technology, 5 Xinmofan Road, Nanjing 210009, People's Republic of China

[2]College of Science, Nanjing University of Technology, 5 Xinmofan Road, Nanjing 210009, People's Republic of China

S. Lu and F. Luo contributed equally to this article.

Correspondence to: H. Huang (E-mail: biotech@njut.edu.cn)

ABSTRACT: Hybrid nanoparticles composed of polydiacetylene (PDA) and magnetite (Fe_3O_4) were fabricated by a double-emulsion method. The structure and composite form of the hybrid nanoparticles were investigated with transmission electron microscopy, scanning electron microscopy, Fourier transform infrared spectroscopy, and dynamic light scattering. The successful incorporation of magnetism to an attractive class of colorimetric PDA sensors was demonstrated. Compared with the PDA vesicles, the hybrid nanoparticles showed better colloidal stability with ethanol stimuli. In this study, we explored the colorimetric sensing ability of the hybrid nanoparticles in response to sodium cetyltrimethylammonium bromide (CTAB). The results show a high sensitivity to CTAB with a limit of detection at 30 μM. The biotin–streptavidin interaction was used as a sensing model to test ligand–receptor interactions on the hybrid nanoparticles' response. The concentration dependence of the chromic response was observed with the limit of visual detection at 20 μg/mL. The Fe_3O_4–PDA hybrid nanoparticles might have great potential applications in biosensing because of their advantages, including separation and sensing. © 2014 Wiley Periodicals, Inc. J. Appl. Polym. Sci. **2014**, *131*, 40634.

KEYWORDS: composites; emulsion polymerization; stimuli-sensitive polymers

Received 9 November 2013; accepted 18 February 2014

DOI: 10.1002/app.40634

INTRODUCTION

Conjugated polymers are of immense scientific and technological interest for a broad spectrum of applications, particularly in optoelectronic and sensing materials.[1] Among the many existing conjugated polymers with physical, chemical, and optical functionalities, polydiacetylene (PDA) is a unique conjugated polymer that shows a significant chromatic change in response to a variety of external stimuli, such as temperature,[2] pH,[3] and particular molecules.[4] PDAs are normally prepared by UV- (254 nm) or γ-ray-induced polymerization of self-assembled diacetylene monomers. The produced polymer exhibits an intense blue color because of electronic delocalization within the conjugated framework; this gives rise to an absorption around 650 nm in the visible region of the electromagnetic spectra.[5] With an external stimulus, a chromatic shift occurs, and this results in a blue–red color transition and an induction of weak fluorescence. Because of these attractive properties, PDA-based sensors have been explored in various fields, including DNA,[6] temperature,[2] trinitrotoluene,[7] prostate specific antigens,[8] cholera toxins, and proteins.[9]

PDA sensors are generally classified into liquid-phase sensors and solid-phase sensors. Liquid-phase sensors are simply prepared and feasibly applied in most cases of biosensing.[9] However, the uses of liquid-phase sensors are limited because of its relative instability, especially because they aggregated easily in response to external stimuli and because of the time-consuming dialysis needed to wash out residual unconjugated receptors. Recently, an innovation was promoted in which solid-phase PDA sensors were prepared by the immobilization of PDA sensors on the surface of substrate.[10] In such advancements, residual unconjugated receptors can be directly washed out instead of being washed out by time-consuming dialysis. There is a lingering problem in the loss of PDA liposomes due to instable immobilization. Recently, multifunctional magnetic nanoparticles have been attracting increased research efforts because they can easily combine the specific functionality of their constituent parts and perform several tasks in parallel.[11] For an example, fluorescent–magnetic hybrid nanoparticles have been of particular interest in the development of diagnostic and therapeutic materials.[12] Magnetic nanoparticles exhibit versatile optical properties as their characteristics can be tuned by

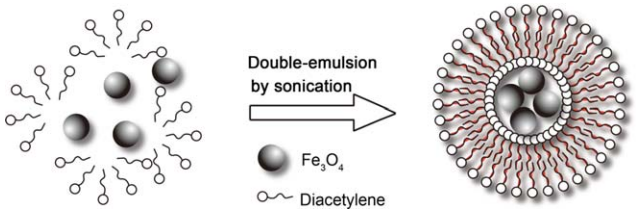

Scheme 1. Schematic representation of the Fe_3O_4–PDA hybrid vesicle. [Color figure can be viewed in the online issue, which is available at wileyonlinelibrary.com.]

changes in the constituent polymer to create polymer blends and by their doping with other dyes. Green et al.[13] incorporated superparamagnetic iron oxide nanoparticles into conjugated polymer micelles to create magnetic–fluorescent semiconducting polymer nanospheres. However, few studies have reported on PDA nanoparticles for loading the magnetic nanoparticles. If hybrid nanoparticles are magnetically responsive, in line with their chromatic response to external stimuli, magnetite (Fe_3O_4) labeling would provide a beneficial feature of enabling rapid isolation and purification of PDA supramolecules and, thus, overcome time-consuming dialysis or often ineffective centrifugation processes. Currently, Lee et al.[14] reported the generation of magnetically responsive PDA/magnetic nanocomposites. In their study, the carboxylic acid group of a PDA vesicle served as the ligand to couple with the Fe_3O_4 nanoparticle surface. In most cases, the chromatic change in response to molecular recognition processes happened on the surface of PDAs, which conjugated with the receptor through the functional group (COOH).[15,16] PDA/magnetic nanocomposites in which carboxylic acid serves as the ligand might result in functional group (COOH) occupation and steric hindrance.

In this study, we investigated the incorporation of Fe_3O_4 nanoparticles into PDA nanoparticles to create multifunctional hybrid nanocomposites. Scheme 1 illustrates the preparation of the Fe_3O_4-nanoparticle-loaded diacetylene nanoparticles with a double-emulsion method. In this study, we investigated the colorimetric sensing ability of hybrid nanoparticles in response to sodium cetyltrimethylammonium bromide (CTAB) and streptavidin.

EXPERIMENTAL

Materials

Iron(III) chloride hexahydrate ($FeCl_3{\cdot}6H_2O$), 10,12-pentacosadiynoic acid, 1-ethyl-3-(3-dimethylaminopropyl) carbodiimide (EDC), *N*-hydroxysuccinimide (NHS), and CTAB were purchased from Sigma. D-Biotin and streptavidin were purchased from Aladdin Reagents (Shanghai, China). Trisodium citrate, ethylene glycol, sodium acetate, and all of the other chemicals used in this study were obtained from Sinopharm Chemical Reagent Co., Ltd. (China). 2,2-(Ethylene dioxy)-bisethylamine (EDEA) were purchased from Entergy Chemical (Shanghai, China).

Synthesis of the Iron Oxide Magnetic Nanoparticles

In a typical fashion, $FeCl_3{\cdot}6H_2O$ (3.25 g) and trisodium citrate (1.3 g) were first dissolved in ethylene glycol (100 mL). Afterward, sodium acetate (6.0 g) was added with stirring. The mixture was stirred vigorously for 30 min and then sealed in a Teflon-lined stainless-steel autoclave (with a 200-mL capacity). The autoclave was heated at 200°C and maintained their for 10 h. It was then allowed to cool to room temperature. The black products were washed with ethanol and deionized water several times and dried *in vacuo* at 50°C to obtain the dried Fe_3O_4 powder.

Fabrication of the Fe_3O_4–PDA Hybrid Nanocomposites

The Fe_3O_4-loaded hybrid nanoparticles (NPs) were prepared with a double-emulsion method based on a modified previous study.[17] In a typical manner, 10,12-pentacosadiynoic acid (PDA) was dissolved in chloroform and passed through a 0.45-μm nylon filter before use. Then, 0.2 mL of a water solution containing 4 mg of Fe_3O_4 NPs was added dropwise into 2-mL chloroform solution containing 20 mg of PDAs under sonication on ice (400 W, 2 min). This primary emulsion was emulsified by sonication on ice in 4 mL of a 0.1% PVA aqueous solution. Subsequently, the resulting water-in-oil-in-water emulsion was diluted by its mixture with 40 mL of a 0.5% PVA aqueous solution under vigorous stirring. After 2 min, the chloroform solvent was evaporated with a rotary evaporator. The Fe_3O_4-loaded vesicles that formed were then centrifuged; after the supernatant was discarded, the vesicles were resuspended in 40 mL of a water solution.

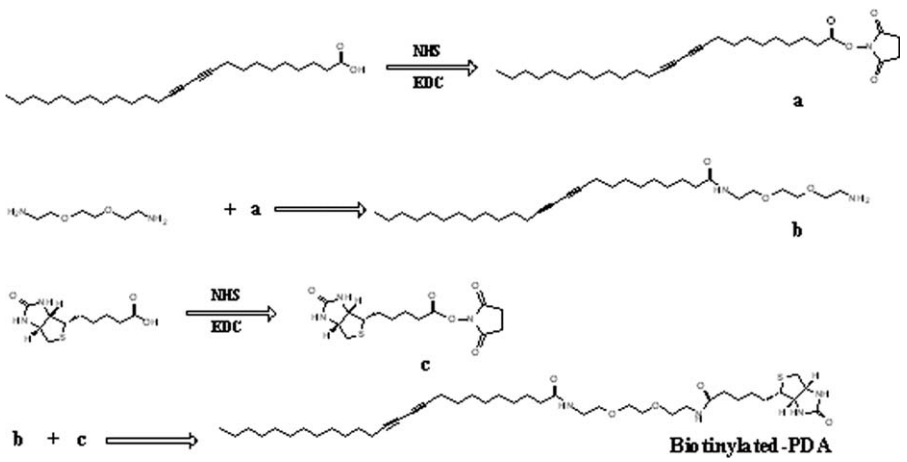

Scheme 2. Synthetic route of PDA–biotin.

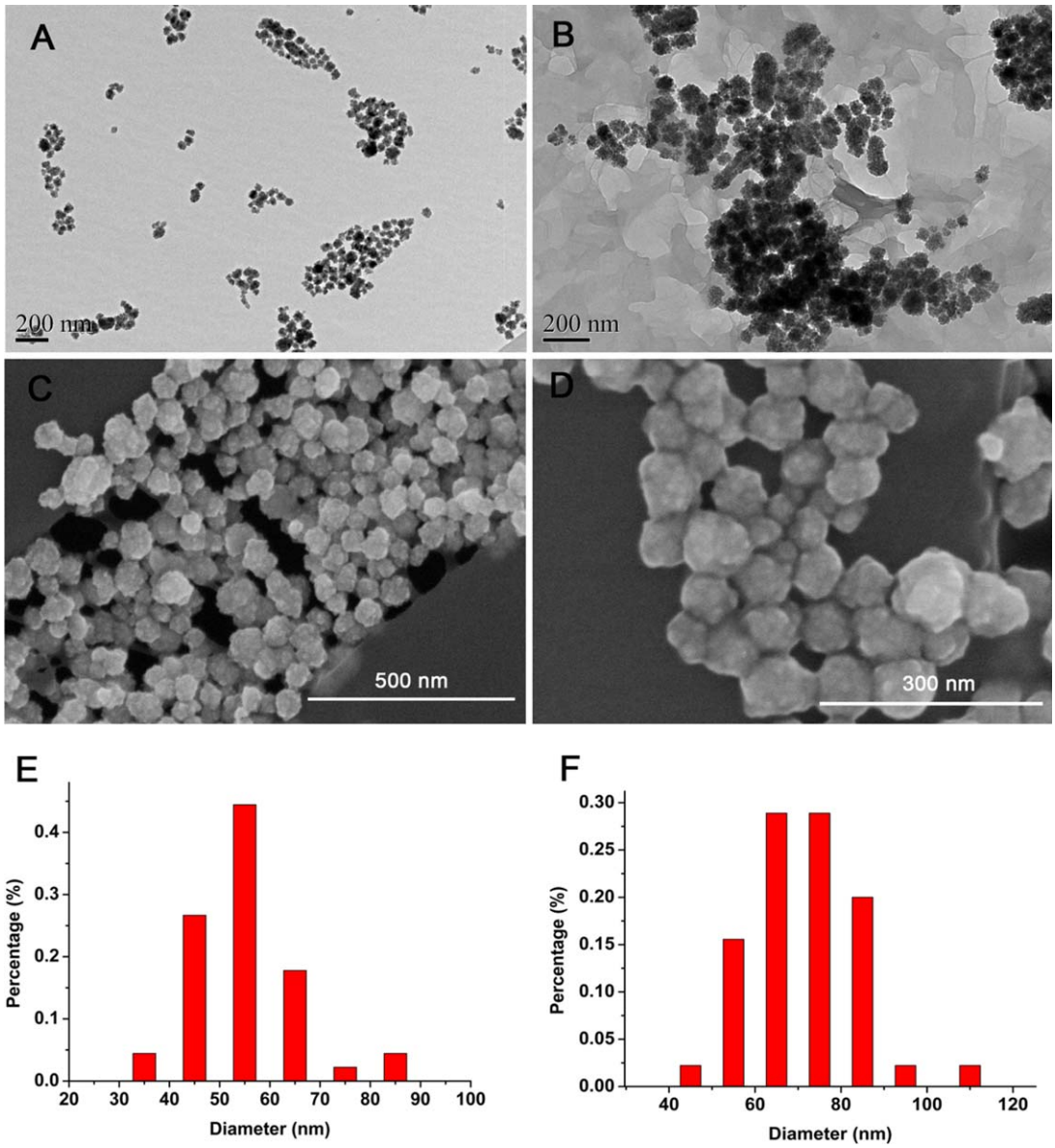

Figure 1. TEM images, SEM images, and DLS for the Fe_3O_4–PDA hybrid vesicles. [Color figure can be viewed in the online issue, which is available at wileyonlinelibrary.com.]

Synthesis of the Biotinylated PDA (Scheme 2)

The biotinylated lipid was synthesized according to a process from the literature[18] via a four-step route outlined in Scheme 2. To a solution of PDA (0.267 g, 0.713 mmol) in dry CH_2Cl_2 (10 mL), NHS (0.0914 g, 0.786 mmol) was added. Then, EDC (0.144 g, 0.713 mmol) was added. The solution was stirred at room temperature for 2 h. This was followed by the rotary evaporation of the CH_2Cl_2. The residue was extracted with diethyl ether and washed with water three times. The organic layer was dried with $MgSO_4$ for 0.5 h and then filtered. The solvent was removed by rotary evaporation to give a white solid powder a (yield = 91%).

A solution of powder a (1.67 g, 3.39 mmol) in 20 mL of dry CH_2Cl_2 was added to EDEA (17 mmol) in 25 mL of CH_2Cl_2 dropwise with vigorous stirring. Three drops of triethylamine were then added. The progress of the reaction was monitored by thin-layer chromatography. After a few hours, the solvent and excess residual amine were evaporated. The residue was extracted with ethyl acetate and then washed with water twice. The organic layer was dried with $MgSO_4$ for 0.5 h, the solution was filtered, and the solvent was removed by rotary evaporation. The product was purified by silica gel chromatography (19:1 $CHCl_3$/methanol) to give 1.0 g of product b as a white solid (54% yield).

To a solution of D-biotin (0.80 g, 3.27 mmol) in dimethylformamide (DMF), NHS (0.38 g, 3.3 mmol) was added; then, EDC (0.67 g, 3.3 mmol) was added. The reaction was stirred overnight, and the solvent DMF was evaporated *in vacuo*. The residue was washed with water and methanol several times to get a white solid c (63% yield).

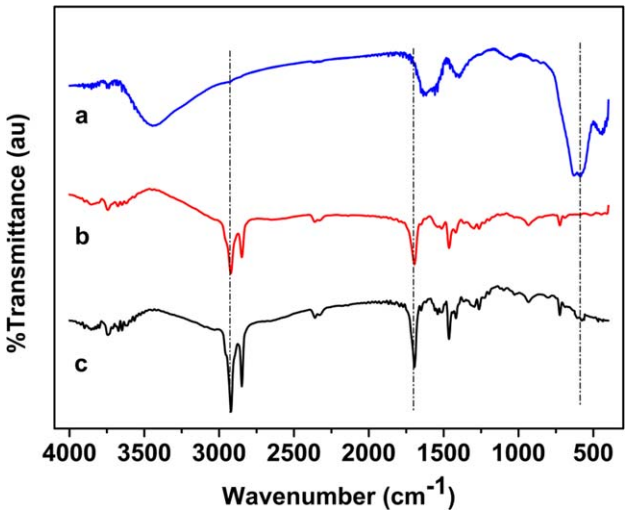

Figure 2. FTIR spectra of the (a) Fe_3O_4, (b) PDA monomer, and (c) Fe_3O_4–PDA hybrid nanoparticles. [Color figure can be viewed in the online issue, which is available at wileyonlinelibrary.com.]

A 0.5 g (0.98 mmol) portion of b was dissolved in a mixture of 20 mL of DMF and 15 mL of CH_2Cl_2. Four drops of triethylamine and 0.33 g (0.98 mmol) of c were dissolved in 10 mL of dry DMF. This mixture was added dropwisely to the solution of b. The mixture was stirred overnight. The progress of the reaction was monitored by thin-layer chromatography. The biotinylated PDA (PDA–biotin) product was isolated after precipitation and washed several times with DMF and diethyl ether with a 65% yield. The product was used without further purification.

Colorimetric and Spectrophotometric Detection of CTAB and Streptavidin

In a typical experiment, a 1-mL reaction solution was prepared by the placement of 500 μL of the synthesized hybrid nanocomposites solution (PDA monomer or PDA derived monomer, 1 m*M*) into a test tube; the solution was diluted to 0.9 mL with 10 m*M* phosphate-buffered saline (pH 7.4). Then, we added 100 μL of CTAB solution (phosphate-buffered saline, pH 7.4) at different concentrations. The reaction was maintained at room temperature for 30 min. The hybrid nanocomposites containing 1 m*M* biotinylated PDA monomer were prepared as described previously. This was followed by the addition of streptavidin at different concentrations and incubation for 30 min.

Characterization

Transmission electron microscopy (TEM) images were taken on a JEOL 200CX transmission electron microscope. A drop of well-dispersed nanoparticles were placed onto the amorphous carbon-coated 200 mesh copper grid; we then dried the sample at ambient temperature before it was loaded into a microscope. Scanning electron microscopy (SEM) images were taken on the JSM-5900, and the samples were coated with Pt for 15 s before analysis. The size and size distribution of the hybrid nanoparticles were determined by dynamic light scattering (DLS; MASTERSI, Malvern Instruments, Ltd.) with an angle detection at 90°. Fourier transform infrared (FTIR) spectroscopy spectra were obtained on a Nicolet A-370 FTIR spectrometer. The magnetic properties of the microspheres were measured on a LDJ 9600 vibrating sample magnetometer at room temperature. A Mettler-Toledo differential scanning calorimetry (DSC) instrument with an FP90 central processor was used to obtain the DSC data of 10-mg precursor, polymer, and composite samples wrapped in a small disk with aluminum foil with heating–cooling–heating cycles in the temperature range from 0 to 200°C at a rate of 10°C/min. A fluorescent microscope (Olympus BX51 W/DP70) was used to observe the PDA vesicles and hybrid nanoparticles images. For analysis of the colorimetric transitions-induced by CTAB and streptavidin, the ultraviolet–visible spectra of the samples were analyzed with an ultraviolet–visible spectrophotometer (PerkinElmer Lambda 25).

RESULTS AND DISCUSSION

Characterization of the PCDA–Fe_3O_4 Hybrid Nanoparticles

The Fe_3O_4-loaded polymeric vesicles were prepared by a double-emulsion method. Figure 1(A) shows the TEM image of the Fe_3O_4 NPs with a size distribution ranging from 30 to 90 nm; this was consistent with SEM images and DLS. Figure 1(B) presents the TEM images of the Fe_3O_4–PDA hybrid nanoparticles. These hybrid nanoparticles formed clusters with diameters ranging from 40 to 120 nm. Figure 1(C,D) shows the SEM images of the Fe_3O_4–PDA hybrid nanoparticles. Compared with the blank Fe_3O_4 [Figure 1(C)], Figure 1(D) clearly reveals that the Fe_3O_4–PDA hybrid nanoparticles were easily aggregated together with a smooth surface. The size and size distribution of the polymeric vesicles were further determined by DLS. The mean diameter of the blank Fe_3O_4 nanoparticles was 55 ± 3 nm, whereas the mean diameter of the Fe_3O_4–PDA nanoparticles was 72 ± 4 nm.

The FTIR spectra of the Fe_3O_4, pure PDAs, and Fe_3O_4–PDA hybrid nanoparticles are shown in Figure 2. The absorption bands at 580 cm^{-1} were assigned to the Fe—O stretching peak from the FTIR spectrum of the Fe_3O_4 particles [Figure 2(a)]. The FTIR spectra of the PDAs [Figure 2(b)] showed lines at 2625 and 2948 cm^{-1} due to the asymmetric and symmetric stretching vibrations, respectively, of the CH_2 groups of the PDA side chains.[19] The lines at 1465 and 1697 cm^{-1} were assigned to the CH_2 scissoring vibrations and hydrogen-bonded carbonyl C=O stretching vibrations.[14,20] As shown in Figure 2(c), these peaks were observed in the FTIR spectra of the Fe_3O_4–PDA hybrid nanoparticles; this contributed to the magnetic nanoparticles being well loaded onto the PDA nanoparticles.

DSC measurements were performed to provide further understanding of the nature of the Fe_3O_4–PDA nanocomposites. The heating scan for the pure PDA monomer [Figure 3(a)] showed an endothermic peak at 69°C due to melting. The heating scan for polydiacetylene [Figure 3(b)] showed a lower endothermic peak at 69°C due to the melting of the unpolymerized monomer. The heating scan for the Fe_3O_4–PDA hybrid nanoparticles [Figure 3(c)] showed an endotherm at 73°C (>69°C). This shift might have demonstrated the strong bonding between the side-chain —COOH head groups and Fe ions.

Magnetic Response and Stability

A suspension of Fe_3O_4–PDA hybrid nanoparticles was generated by 254-nm UV irradiation. Figure 4 clearly shows that the

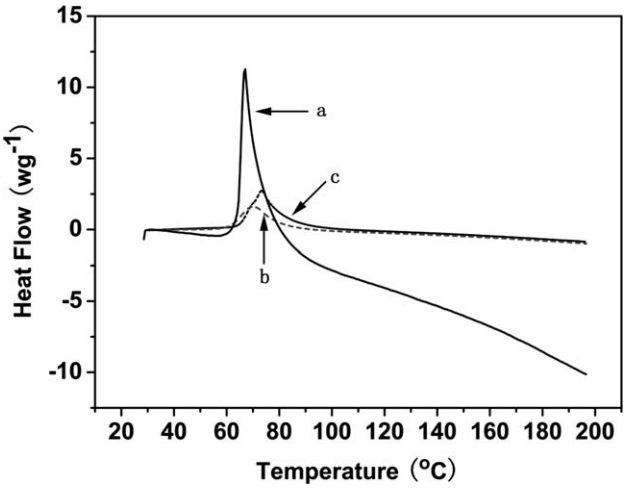

Figure 3. DSC heating scans for the (a) PDA monomer, (b) polyPDA, and (c) Fe_3O_4–PDA hybrid nanoparticles.

appearance of the indigo suspension was generated after UV irradiation; this demonstrated that the hybrid nanoparticles were successfully polymerized and potentially applied in biosensing and imaging. Magnetic characterization at 300 K with a vibrating sample magnetometer showed that the saturation magnetization values of the Fe_3O_4 and Fe_3O_4–PDA hybrid were 60.5 and 51.4 emu/g [Figure 4(A)]. The polymerized or unpolymerized Fe_3O_4–PDA hybrid nanoparticles could be aggregated very quickly when they were exposed to an external magnetic field [Figure 4(B)]. These hybrid nanoparticles were also well dispersed with vigorous shaking and sonication, and this finally resulted in a homogeneous suspension when the external magnetic field was removed. These results show that the polymerized and unpolymerized Fe_3O_4–PDA hybrid nanoparticles possessed excellent magnetic responsivity and redispersability; this was important in terms of their practical manipulation.

Figure 5 shows the fluorescence microscopy images of the PDA vesicles and the Fe_3O_4–PDA hybrid nanoparticles with ethanol stimuli. As shown in Figure 5(A), ethanol addition to the PDA vesicle solution resulted in rapid aggregation. As compared with the case of the PDA vesicles, the hybrid nanoparticles showed good dispersion after ethanol addition [Figure 5(B)]. These results indicate the PDA supermolecules embedded with Fe_3O_4 reduced aggregation but maintained good dispersion upon external stimuli.

Chromatic Response to the CTAB Stimuli

It is well known that the PDA vesicle solution exhibits an intense chromatic transition from blue to red with the addition of surfactants, such as SDS, CTAB, and Triton X-100.[21,22] To investigate its ability to sense surfactants for hybrid nanoparticles, in this study, we observed the colorimetric transitions from the hybrid nanoparticle solution in response to CTAB. The UV absorption spectra of the hybrid nanoparticle solution with CTAB stimuli are shown in Figure 6(A). As the concentration of CTAB was increased (0, 30, 60, 90, and 120 μM), we observed decreases in the absorbances at 650 and 600 nm. However, the absorbance at 540 nm increased without regularity. Generally, the colorimetric response (%CR) value is used to quantify the sensitivity of the PDA vesicles with external stimuli on the premise of a decrease in the blue phase (650 nm) concurrent with an increase in the red phase (540 nm).[23] Hence, to quantify the sensitivity of the hybrid nanoparticle colorimetric sensor, we used the value of the absorption spectra at 600 nm to generate a calibration curve. With this metric, we estimated the limit of visual detection of this sensor at 30 μM [Figure 6(B)] with $R^2 = 0.98$; this was than that of the pure PDA vesicle system in a previous study (0.5 mM).[21]

Chromatic Response to Specific Ligand–Receptor Interactions

The PDA vesicles exhibited dramatic colorimetric changes from blue to red after stress was externally applied. This stress presumably originated from the interactions between a receptor attached to PDA and ligands in solution and resulted in changes in the effective conjugation length marked by a color change of the liposome solution. The ligand–receptor interaction PDA system is the most common type of recognition in biosensing systems.[24] Biotin–streptavidin chemistry has been well-studied in

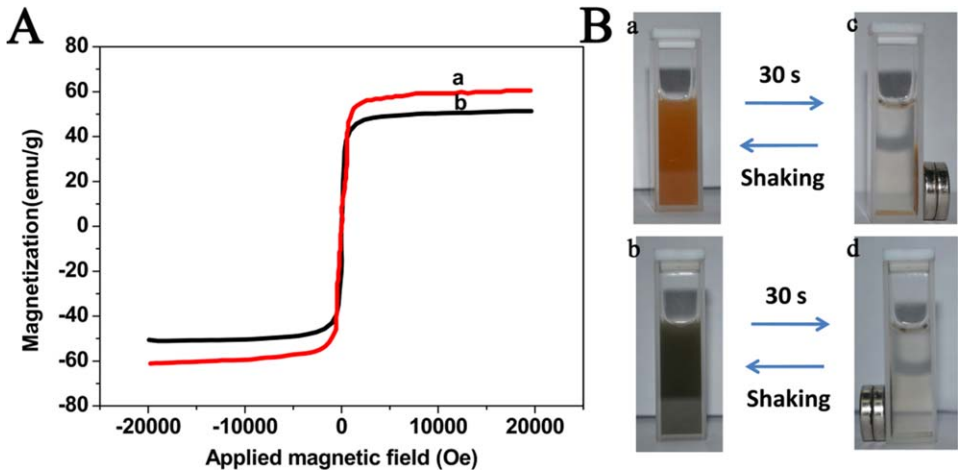

Figure 4. (A) Room-temperature (300 K) magnetic hysteresis loops of the (a) Fe_3O_4 and (b) Fe_3O_4–PDA hybrid. (B) Magnetic separation–redispersion process of (a,c) unpolymerized Fe_3O_4–PDA and (b,d) polymerized Fe_3O_4–PDA. [Color figure can be viewed in the online issue, which is available at wileyonlinelibrary.com.]

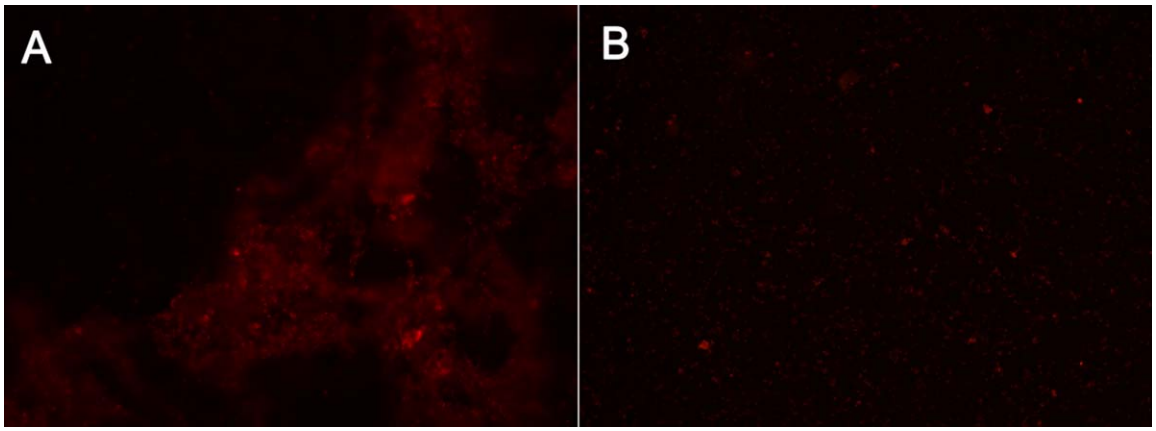

Figure 5. Fluorescent microscopy images of the (A) PDA vesicles and (B) Fe_3O_4–PDA hybrid nanoparticles on the addition of ethanol (ethanol concentration = 30%). [Color figure can be viewed in the online issue, which is available at wileyonlinelibrary.com.]

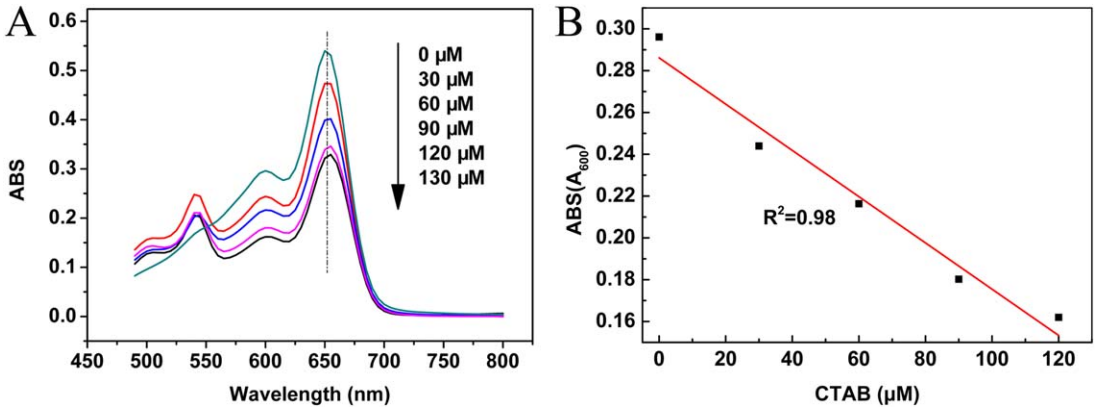

Figure 6. (A) Absorption spectra of the hybrid nanoparticle solution in response to different amounts of CTAB and (B) response curves of CTAB. For all of the response curves, the absorption wavelength was 600 nm. [Color figure can be viewed in the online issue, which is available at wileyonlinelibrary.com.]

the literature, and it has been used for many biomedical applications because of its extremely strong interactions and the commercial availability of many biotin- and streptavidin-tagged probes.[25] In this study, we investigated the effect of molecular interactions between biotin receptors (conjugated PDA head groups) and streptavidin on the hybrid vesicle sensor response. We began to synthesize PDA–biotin first and then engineered the Fe_3O_4–PDA–biotin hybrid nanoparticles.

As shown in Scheme 2, the biotin–NHS was obtained according to a procedure from a previous study.[18] As shown in Figure 7 and Table I, the representative FTIR spectra of biotin showed a band peaking near 1683 cm^{-1}, which was assigned to biotin ureido carbonyl stretching.[26] For biotin–NHS, the band at 3325 cm^{-1} was assigned to biotin COOH streching.[27] Bands at 1072, 1217, 1575, and 1819 cm^{-1} were assigned to C—H deformations on NHS, C—N—C stretching-mode NH deformation on NHS, NH deformation with C—N stretching, and NHS ester, respectively.[26,28,29] The spectra of biotin–NHS also showed bands appearing at 3325, 1683, and 650 cm^{-1}, which contributed to the features of the spectra of biotin. The feature that was common to PDA–biotin and PDA was the band near 2928

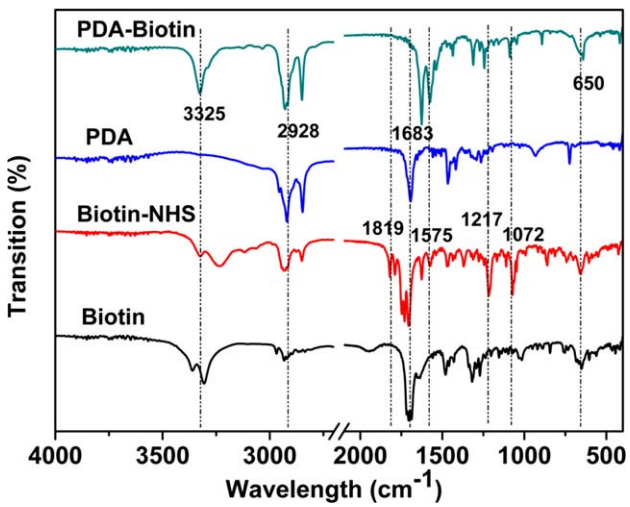

Figure 7. Representative FTIR spectra of biotin, biotin–NHS, PDA, and PDA–biotin. [Color figure can be viewed in the online issue, which is available at wileyonlinelibrary.com.]

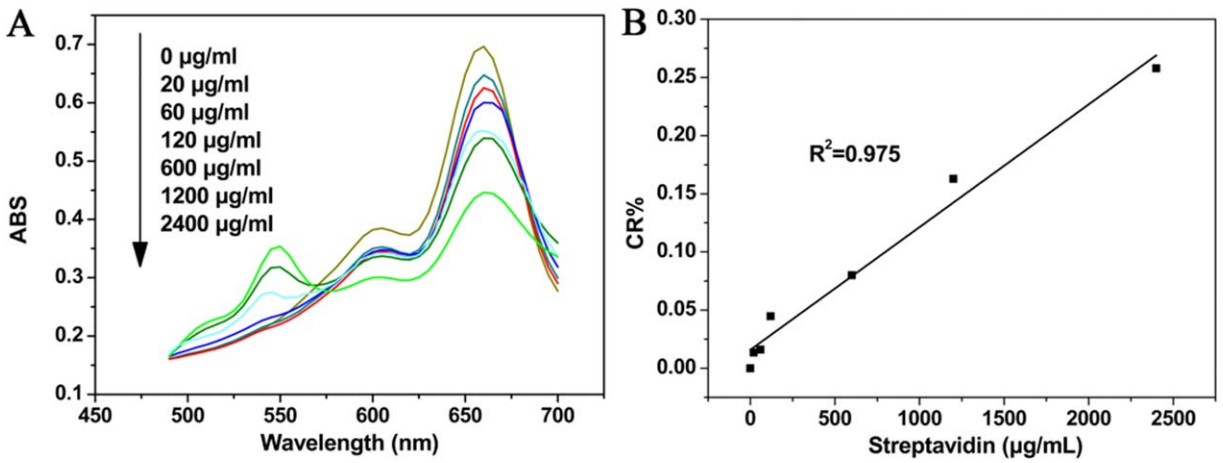

Figure 8. (A) Absorption spectra of the hybrid nanoparticles in response to different amounts of streptavidin and (B) response curves of streptavidin quantified by CR%. [Color figure can be viewed in the online issue, which is available at wileyonlinelibrary.com.]

cm^{-1}, which was assigned to CH_2 stretching mode in the PDA backbone.[19] The features that were common to PDA–biotin and biotin–NHS were bands at 650, 1072, 1575, and 3325 cm^{-1}. The features of the spectra for NHS disappeared in the spectra of PDA–biotin, including bands at 1217 and 1819 cm^{-1} (assigned to the C—N—C stretching-mode NH deformation on NHS and NHS ester). We noted that the band peaking near 1575 cm^{-1} in the spectrum of PCDA–biotin that became stronger might have been due to NH stretching with EDEA.

The colorimetric changes of the Fe_3O_4–PDA–biotin assemblies in response to varied concentrations of streptavidin [Figure 8(A)] were observed. As the concentration of streptavidin increased (0, 20, 60, 120, 1200, and 2400 μg/mL), we observed a decrease in the absorbance at 660 nm. Only when the streptavidin concentration increased up to 1200 μg/mL did the red phase at 550 nm appear, whereas when the intensity increased, the concentration of streptavidin increased.

Quantification of the extent of the blue–red color transition was given by the %CR, as defined by

$$\%CR = (PB_0 - PB_I)/PB_0$$

Table I. FTIR Band Assignments for Biotin, Biotin–NHS, PDA, and PDA–Biotin

Frequency	Assignments	Reference
650	Not previously noted	
1072	C—H deformations on NHS succinimide ring	25
1217	NHS C—N—C stretching mode	27
1575	Amide II (NH deformation with C—N stretching)	25
1683	Biotin ureido carbonyl stretching; PDA C=O stretching mode	25
1819	NHS ester	28
2928	PDA CH_2 stretching mode	19
3325	Biotin COOH stretching	26

where PB_0 is the blue/red ratio of the control sample [$PB_0 = A_{660}/(A_{660} + A_{550})$] and PB_I is the value obtained for the vesicle solution after the colorimetric transition occurs for the samples [$PB_I = A_{660}/(A_{660} + A_{550})$]. A_{660} and A_{550} represents the absorption at 660 nm and 550 nm, respectively. As shown in Figure 8(B), the addition of 100 μL of 200 μg/mL streptavidin to 900 μL of a Fe_3O_4/PDA–biotin mixture (in response to 20 μg/mL streptavidin) resulted in a 1.4% chromic response. This colorimetric transition indicated that the interaction of streptavidin with PDA–biotin induced changes in the head-group and side-chain organization within the PDA systems and affected the conjugated framework. As the concentration addition of streptavidin increased, the %CR increased; this was in accordance with the concentration dependence of the chromic response previously seen in other PDA-based colorimetric sensors by other research groups.[30] In response to 1200 μg/mL streptavidin, the colorimetric transitions of the reacting solution (CR, 16.3%) turned from blue to red, and this could be easily observed by the naked eye. Using this metric, we estimated the limit of visual detection of this sensor to be 20 μg/mL [Figure 8(B)] with $R^2 = 0.975$; this was similar to the pure PDA vesicle system (10 μg/mL).[19]

CONCLUSIONS

In this study, the Fe_3O_4–PDA hybrid nanoparticles were successfully prepared. These hybrid nanoparticles were stable and dispersed compared with the PDA vesicle system. Simultaneously, they showed a magnetic response because of the successful incorporation of Fe_3O_4. This study demonstrated the high colorimetric sensing ability of hybrid nanoparticles with CTAB. Moreover, the biotin–streptavidin interactions were used as a sensing model system to test the special ligand–receptor interaction for hybrid nanoparticle response.

ACKNOWLEDGMENTS

This work was supported by the National Science Foundation for Distinguished Young Scholars of China (contract grant number 21225626), the Key Program of the National Natural Science Foundation of China (contract grant number 20936002), and the

Program of International S&T Cooperation (contract grant number 2012DFA51050) and the project of scientific research innovation of Jiangsu province for doctor (CXZZ12-0437).

REFERENCES

1. Thomas, S. W.; Joly, G. D.; Swager, T. M. *Chem. Rev.* **2007**, *107*, 1339.
2. Ryu, S. M.; Yoo, I.; Song, S.; Yoon, B.; Kim, J. M. *J. Am. Chem. Soc.* **2009**, *131*, 3800.
3. Kew, S. J.; Hall, E. A. H. *Anal. Chem.* **2006**, *78*, 2231.
4. Lee, S. W.; Kang, C. D.; Yang, D. H.; Lee, J. S.; Kim, J. M.; Ahn, D. J.; Sim, S. *J. Adv. Funct. Mater.* **2007**, *17*, 2038.
5. Jelinek, R.; Kolusheva, S. *Top. Curr. Chem.* **2007**, *277*, 155.
6. Jung, Y. K.; Kim, T. W.; Kim, J.; Kim, J. M.; Park, H. G. *Adv. Funct. Mater.* **2008**, *18*, 701.
7. Jaworski, J.; Yokoyama, K.; Zueger, C.; Chung, W. J.; Lee, S. W.; Majumdar, A. *Langmuir* **2011**, *27*, 3180.
8. Kwon, K., II.; Kim, J. P.; Sim, S. *J. Biosens. Bioelectron.* **2010**, *26*, 1548.
9. Park, C. H.; Kim, J. P.; Lee, S. W.; Jeon, N. L.; Yoo, P. J.; Sim, S. *J. Adv. Funct. Mater.* **2009**, *19*, 3703.
10. Lee, J. S.; Kim, H. J.; Kim, J. S. *J. Am. Chem. Soc.* **2008**, *130*, 5010.
11. Hao, R.; Xing, R. J.; Xu, Z. C.; Hou, Y. L.; Gao, S.; Sun, S. H. *Adv. Mater.* **2010**, *22*, 2729.
12. Mulder, W. J. M.; Griffioen, A. W.; Strijkers, G. J.; Cormode, D. P.; Nicolay, K.; Fayad, Z. A. *Nanomedicine* **2007**, *2*, 307.
13. Howes, P.; Green, M.; Bowers, A.; Parker, D.; Varma, G.; Kallumadil, M.; Hughes, M.; Warley, A.; Brain, A.; Botnar, R. *J. Am. Chem. Soc.* **2010**, *132*, 9833.
14. Lee, J.; Yoon, B.; Ham, D. Y.; Yarimaga, O.; Lee, C. W.; Jaworski, J.; Kim, J. M. *Macromol. Chem. Phys.* **2012**, *213*, 893.
15. Lee, K. M.; Moon, J. H.; Jeon, H.; Chen, X. Q.; Kim, H. J.; Kim, S.; Kim, S. J.; Lee, J. Y.; Yoon, J. *J. Mater. Chem.* **2011**, *21*, 17160.
16. Yarimaga, O.; Jaworski, J.; Yoon, B.; Kim, J. M. *Chem. Commun.* **2012**, *48*, 2469.
17. Wei, Q.; Li, T.; Wang, G. L.; Li, H.; Qian, Z. Y.; Yang, M. H. *Biomaterials* **2010**, *31*, 7332.
18. Li, X. L.; Kohli, P. *J. Phys. Chem. C* **2010**, *114*, 6255.
19. Kim, J. M.; Lee, J. S.; Choi, H.; Sohn, D.; Ahn, A. *J. Macromolecules* **2005**, *38*, 9366.
20. Patlolla, A.; Zunino, J.; Frenkelc, A. I.; Iqbal, Z. *J. Mater. Chem.* **2012**, *22*, 7028.
21. Su, Y. L.; Li, J. R.; Jiang, L. *Colloids Surf. B* **2004**, *39*, 113.
22. Su, Y. L.; Li, J. R.; Jiang, L. *Colloids Surf. A* **2005**, *257*, 25.
23. Kolusheva, S.; Shahal, T.; Jelinek, R. *J. Am. Chem. Soc.* **2000**, *122*, 776.
24. Song, Y. J.; Wei, W. L.; Qu, X. G. *Adv. Mater.* **2011**, *23*, 4215.
25. Green, N. M. *Methods Enzymol.* **1990**, *184*, 51.
26. Lapin, N. A.; Chabal, Y. J. *J. Phys. Chem. B* **2009**, *113*, 8776.
27. Bunaciu, A. A.; Bacalum, E.; Aboul-Enein, H. Y.; Udristioiu, G. E.; Fleschin, S. *Anal. Lett.* **2009**, *42*, 1321.
28. McKittrick, P. T.; Keaton, J. E. *Appl. Spectrosc.* **1990**, *44*, 812.
29. Frey, B. L.; Corn, R. M. *Anal. Chem.* **1996**, *68*, 3187.
30. Reppy, M. A.; Pindzola, B. A. *Chem. Commun.* **2007**, 4317.